JOURNAL OF THERMOPHYSICS AND HEAT TRANSFER
Vol. 10, No. 3, July–September 1996

# Natural Convection in the Annulus Between Concentric Horizontal Circular and Square Cylinders

F. Moukalled*
*American University of Beirut, Beirut, Lebanon*
and
S. Acharya†
*Louisiana State University, Baton Rouge, Louisiana 70803*

**Numerical solutions are presented for natural convection heat transfer between a heated horizontal cylinder placed concentrically inside a square enclosure. Three different aspect ratios ($R/L$ = 0.1, 0.2, and 0.3), and four different Rayleigh numbers ($Ra$ = $10^4$, $10^5$, $10^6$, and $10^7$), are considered. The governing elliptic conservation equations are solved in a boundary-fitted coordinate system using a control volume-based numerical procedure. Results are displayed in the form of streamlines, isotherms, maximum stream function estimates, and local and average normalized Nusselt number values. At constant enclosure aspect ratio, the total heat transfer increases with increasing Rayleigh number. For constant Rayleigh number values, convection contribution to the total heat transfer decreases with increasing values of $R/L$. For convection-dominated flows, the average Nusselt number correlation is expressed as $\overline{Nu} = 0.92Ra^{0.23}(R/L)^{0.57}$. Generated results are in good agreement with previously published experimental and numerical data.**

## Nomenclature

$A$ = surface area for heat transfer
$c_p$ = specific heat of fluid
$h$, $\bar{h}$ = local and average convection heat transfer coefficient, $\bar{h} = Q_{\text{conv}}/A(T_i - T_o)$
$k$ = thermal conductivity
$L$ = width of cavity
$Nu$, $\overline{Nu}$ = local and average Nusselt number, $\overline{Nu} = \bar{h}_i s_{i,\max}/k$, $\overline{Nu} = \bar{h}_o s_{o,\max}/k$, $\overline{Nu}_L = \bar{h}L/k$
$Pr$ = Prandtl number, $\mu c_p/k$
$p$, $P$ = thermodynamic pressure and dimensionless pressure
$Q_{\text{conv}}$ = total heat transfer from the surface
$R$ = radius of cylinder
$Ra$ = Rayleigh number, $g\beta(T_h - T_c)L^3/\nu\alpha$
$s_i$, $s_o$ = distance along the inner and outer enclosure surfaces
$T$ = dimensional temperature
$T_c$ = temperature of the outer cold surface
$T_h$ = temperature of the inner heated surface
$u$, $U$ = dimensional and dimensionless velocity in $x$ direction
$v$, $V$ = dimensional and dimensionless velocity in $y$ direction
$x$, $X$ = dimensional and dimensionless coordinate along the horizontal direction
$y$, $Y$ = dimensional and dimensionless coordinate along the vertical direction
$\theta$ = dimensionless temperature
$\mu$ = dynamic viscosity
$\nu$ = kinematic viscosity
$\xi$, $\eta$ = transformed coordinate
$\rho$ = density
$\psi$ = stream function

*Subscripts*
$i$ = heated inner surface
$o$ = cooled outer surface

Received May 10, 1995; revision received Jan. 16, 1996; accepted for publication Jan. 29, 1996. 
*Associate Professor, Department of Mechanical Engineering.
†Professor, Department of Mechanical Engineering.

## Introduction

MANY investigations on natural convection heat transfer in enclosures have been reported in recent years because of the growing need for a better understanding of this phenomenon in nuclear safety design and electronic packaging. However, most of the numerical and experimental work in this area has concentrated on natural convection in isothermal horizontal cylindrical or spherical annuli. Comparatively, little work has been done on natural convection heat transfer in a more complex annuli. In this study, natural convection in the annuli between an inner circular body and an outer rectangular enclosure is investigated.

Natural convection heat transfer in a horizontal cylindrical annulus has been extensively studied. Kuehn and Goldstein[1] presented experimental and numerical results for such an annulus together with an extensive review of the previous research done in the area. Custer and Shaughnessy[2] obtained numerical results for natural convection of liquid metals in a cylindrical annulus. Results for turbulent natural convection using a $k$-$\varepsilon$ turbulence model were reported by Farouk and Guceri.[3] The effect of conduction along the walls of the cylindrical annulus on the unsteady natural convection was studied by Bubnovich and Kolesnikov[4] and Kolesnikov and Bubnovich.[5] A comprehensive numerical study of natural convection in horizontal annuli for a wide range of Rayleigh numbers and diameter ratios was performed by Kumar.[6]

Natural convection heat transfer from a square cylinder placed in a cylindrical enclosure was reported by Chang et al.[7] More recently, Oosthuizen and Paul[8] reported results for natural convection from a prismatic cylinder in a square enclosure. Experimental studies of natural convection heat transfer between concentrically-mounted bodies (spheres, cylinders, and cubes), and their spherical and cubical enclosures, were reported by Warrington and Powe[9] at moderate Rayleigh numbers, and by Warrington et al.[10] at low Rayleigh numbers. In both studies, correlations between Nusselt number and Rayleigh number were presented and the effect of the enclosure

shape was seen to be small, as long as the appropriate length scale was employed.

The intent of this article is to numerically study the details of natural convection heat transfer of air in the annulus between an isothermal heated inner cylinder and an isothermal cooled rectangular enclosure. Ghaddar[11] recently reported calculations of natural convection around a cylindrical rod placed in an enclosure with a hydraulic diameter that is nearly 40 times the cylinder diameter. Their results were in good qualitative agreement with the published data of Warrington and Powe.[9] However, there were significant quantitative differences between the two results, because of the large annulus gap in the study of Ghaddar.[11] In this article results are reported for a geometry that is more representative of an annulus, with dimensionless gap widths in the range of 3–10. A review of the literature reveals that such a configuration has not yet been studied.

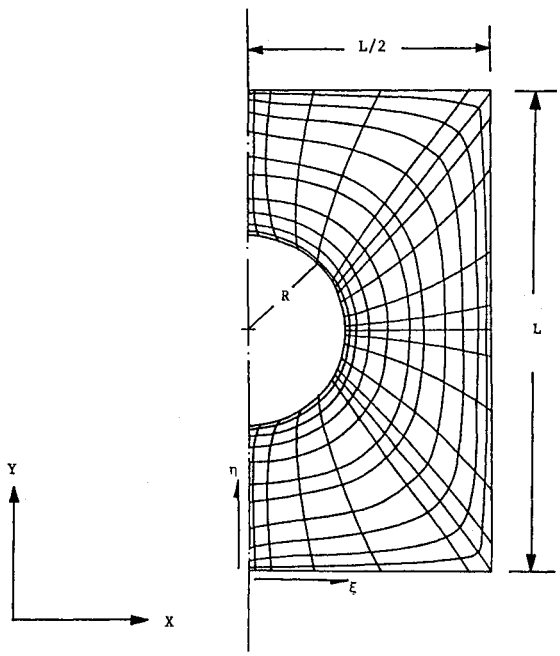


**Fig. 1 Physical domain and an illustrative grid network generated.**

## Governing Equations

The governing equations are solved for only one-half of the physical domain (Fig. 1) since the flow is symmetric about the vertical axis. The outer cooled square cylinder and the heated inner circular cylinder are maintained at temperatures $T_o$ and $T_i$, respectively. The flow is considered to be steady, laminar, and two dimensional, and the fluid properties are assumed to be uniform except for the density. The variation of density with temperature is modeled using the Boussinesq approximation and is therefore considered only in the body force term appearing in the momentum equation. The governing equations are nondimensionalized using the following definitions of nondimensional variables:

$$X = x/L, \qquad Y = y/L \tag{1}$$

$$U = uL/\nu, \qquad V = vL/\nu \tag{2}$$

$$P = (p + \rho g y)/\rho(\nu/L)^2 \tag{3}$$

$$\theta = (T - T_o)/(T_i - T_o)$$

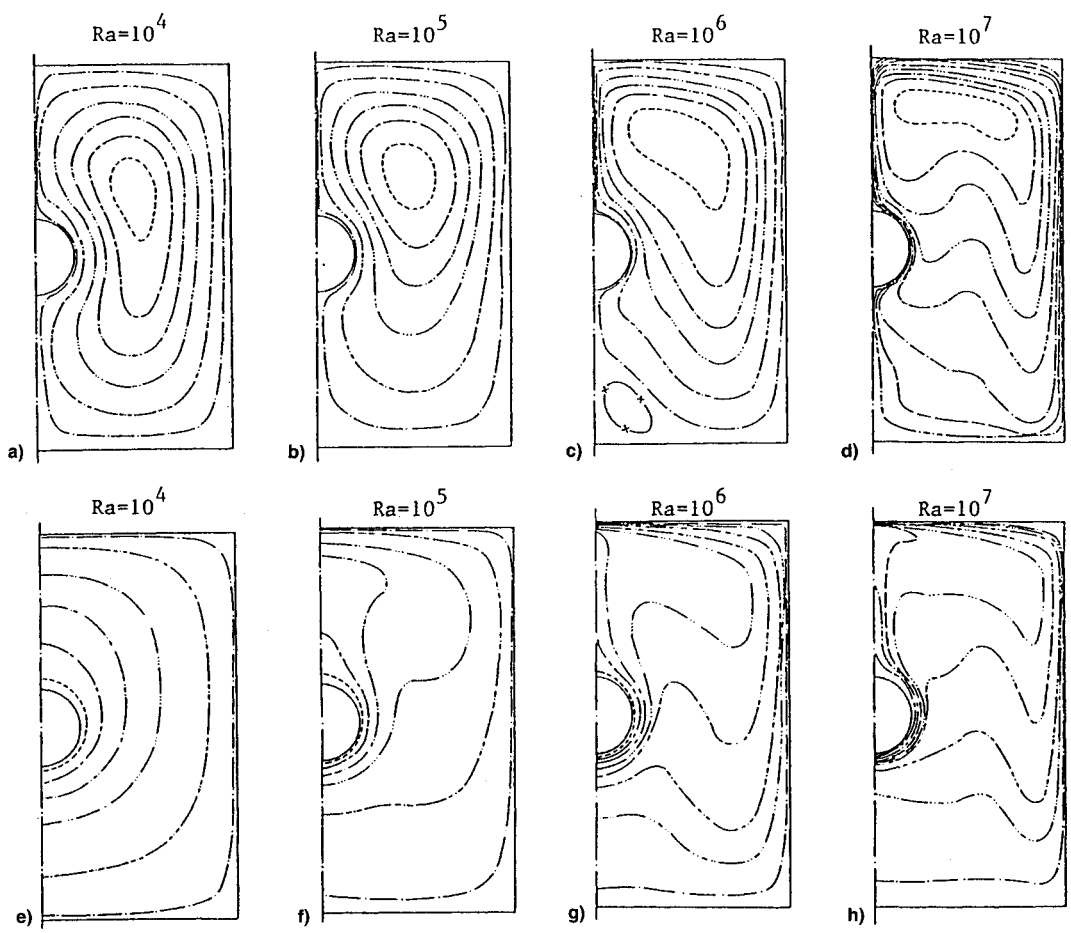


**Fig. 2 Streamline and isotherm plots ($R/L$ = 0.1).**

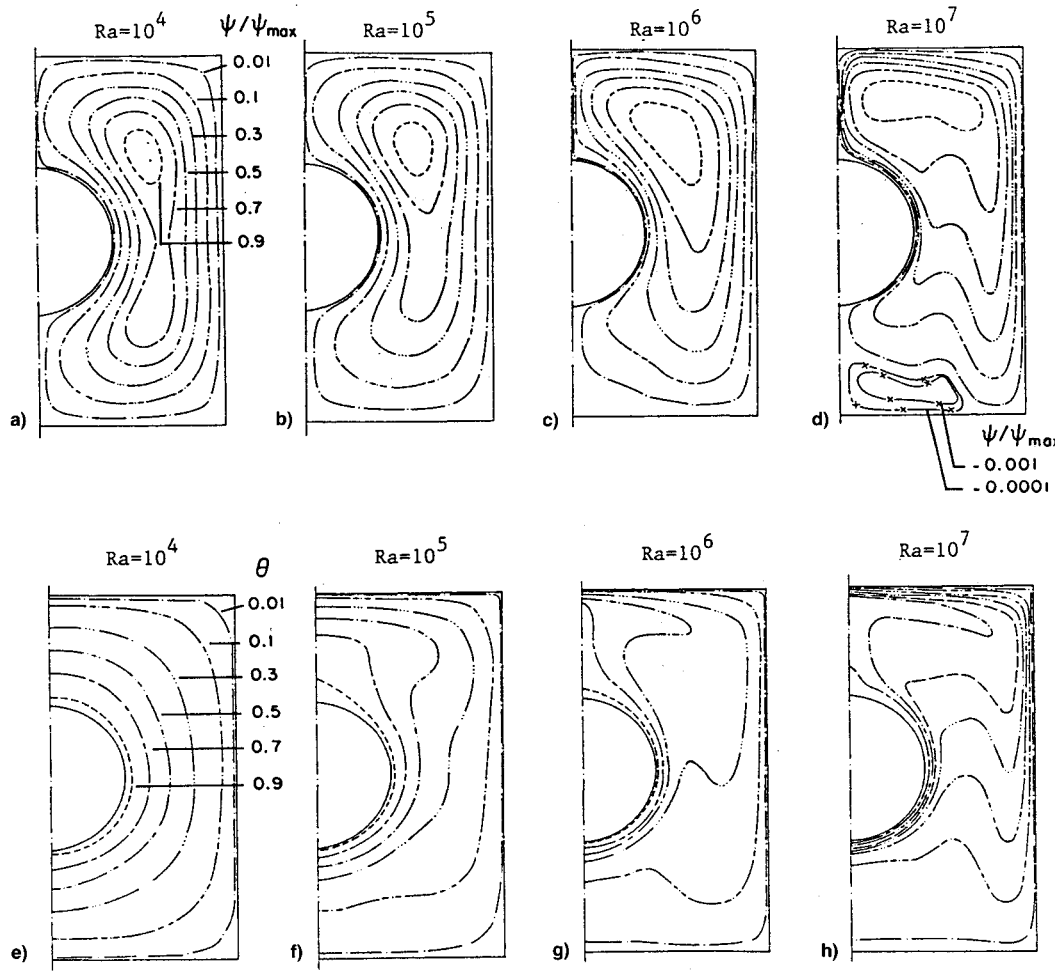


**Fig. 3 Streamline and isotherm plots ($R/L$ = 0.2).**

With the previously mentioned assumptions, the nondimensional mass, momentum, and energy equations become

$$\frac{\partial U}{\partial X} + \frac{\partial V}{\partial Y} = 0 \tag{4}$$

$$U\frac{\partial U}{\partial X} + V\frac{\partial U}{\partial Y} = -\frac{\partial P}{\partial X} + \frac{\partial^2 U}{\partial X^2} + \frac{\partial^2 U}{\partial Y^2} \tag{5}$$

$$U\frac{\partial V}{\partial X} + V\frac{\partial V}{\partial Y} = -\frac{\partial P}{\partial Y} + \frac{\partial^2 V}{\partial X^2} + \frac{\partial^2 V}{\partial Y^2} + \frac{Ra\theta}{Pr} \tag{6}$$

$$U\frac{\partial \theta}{\partial X} + V\frac{\partial \theta}{\partial Y} = \frac{1}{Pr}\left(\frac{\partial^2 \theta}{\partial X^2} + \frac{\partial^2 \theta}{\partial Y^2}\right) \tag{7}$$

For the parameter ranges considered in this study ($Ra \leq 10^7$, $Pr = 0.71$), the assumption of steady-state flow is justified. Warrington and Powe,[9] in their experimental study, and Ghaddar,[11] in his unsteady numerical calculations, both observed steady-state behavior for $Ra$ and $Pr$ numbers similar to those in the present study.

The problem is solved using the no-slip boundary conditions along the walls. The hot inner and cold outer walls are maintained at nondimensional uniform temperatures of 1 and 0, respectively. The $U$-velocity and the gradients of the remaining variables are set to zero along the symmetry line.

## Solution Procedure

Since the boundaries of the domain do not lie along natural coordinates, a boundary-fitted nonorthogonal coordinate system is used. The solution procedure involves grid generation, discretization of the governing equations, and an algorithm for solving the equations.

### Grid Generation

The curvilinear grid that maps the physical ($X$, $Y$) domain shown in Fig. 1 to a uniform computational ($\xi$, $\eta$) domain is obtained by solving a set of Poisson equations relating the two coordinates (Ref. 12). The equations for the grid positions are discretized using central differences, and the resulting algebraic system of equations is solved iteratively by a block–tridiagonal Thomas algorithm. The resulting solution gives ($X$, $Y$) values at uniform ($\xi$, $\eta$) values, and all metric quantities can be calculated from this solution.

### Discretization of Conservation Equations

The conservation equations represented by Eqs. (4–7) are transformed from the ($X$, $Y$) space to the ($\xi$, $\eta$) space, through a coordinate transformation. The domain is subdivided into a finite number of control volumes or cells, each associated with a grid point. The governing differential equation is integrated over each control volume and profile approximations (the power-law scheme of Patankar[13] is used here) made in each coordinate direction to approximate the derivatives by algebraic expressions. The resulting system of algebraic equations is then solved by a block-Thomas algorithm.[13] To evaluate the pressure field, a pressure correction $P'$ ($=P - P^*$, where $P^*$ is the solution from the previous iteration) is defined and a pressure correction equation is derived by combining the momentum and continuity equations as in the SIMPLE procedure of Patankar.[13] A collocated grid is used in the present study,

and oscillations in the predicted solutions are suppressed by adding correction terms to the interface mass-flux sources in the pressure-correction equation as suggested by Rhie and Chow.[14] Additional details of the numerical procedure can be found in Patankar[13] and Rhie and Chow.[14]

#### Numerical Accuracy

Computations are performed on a 42 × 35 mesh size. The grid points are unevenly distributed over the domain and concentrated near the walls where higher gradients are expected. The grid independence of the results is verified by obtaining results for a finer grid (62 × 50) and comparing them with the results of the coarser grid (42 × 35). This comparison revealed that the maximum differences were less than 1.9% in the peak Nusselt number value and less than 1.7% in the peak midheight horizontal velocity. Conservation of mass, momentum, and energy was found to be satisfied to within 0.001% in each control volume. As shown later, computed results are also found to be in excellent agreement with published experimental[9] and numerical[6] data.

## Results and Discussion

Parameter values considered are three different aspect ratios ($R/L$ = 0.1, 0.2, and 0.3) and four Rayleigh numbers in the range of $10^4$–$10^7$. Air is considered to be the working fluid and, as previously mentioned, the Prandtl number is fixed at 0.71.

#### Streamlines and Isotherms

The flow patterns and isotherms in the enclosure domain are depicted in Figs. 2–4. The maximum stream function values ($|\psi_{max}|$) are shown in Table 1.

Figures 2 and 3 reveal that, in general, the flow moves up along the heated cylinder and the vertical symmetry line to reach the enclosure top, and then moves radially outwards and down along the cold walls of the enclosure. The eye of the recirculation is situated in the upper portion of the enclosure where the flow is stronger. With increasing Rayleigh number (compare streamlines in Figs. 2a–2d and 3a–3d), the strength of the convective flow increases and the eye of the recirculation eddy moves further upward and outward toward the colder wall. At the higher Rayleigh numbers, the velocities at the bottom of the enclosure are very low compared to the velocities at the middle and top regions. This is indicative of stratification effects in the lower regions of the enclosure.

At a higher $R/L$ value ($R/L$ = 0.3, Fig. 4), the recirculating flow exhibits two vortex cores within one overall rotating eddy (see Figs. 4a–4d). These two inner vortices rotate in the clockwise direction, and as the Rayleigh number increases, the center of the lower vortex moves up and approaches the top vortex until the two vortices merge (Fig. 4d).

At $Ra = 10^7$, and for all aspect ratios considered, the convective flow strength is significant, and the isotherm plots in Figs. 2h, 3h, and 4h clearly show the boundary-layer behavior on the lower part of the heated cylinder and the upper part of the cooled enclosure. At $R/L$ = 0.1, the boundary layer along the inner cylinder separates away from the surface near the

**Table 1 Maximum absolute values of the stream function**

| | $R/L$ | | |
|---|---|---|---|
| $Ra$ | 0.1 | 0.2 | 0.3 |
| $10^4$ | 2.44 | 1.43 | 0.7 |
| $10^5$ | 14.3 | 11.8 | 7.19 |
| $10^6$ | 35.7 | 33.9 | 30 |
| $10^7$ | 65.8 | 64.7 | 64.4 |

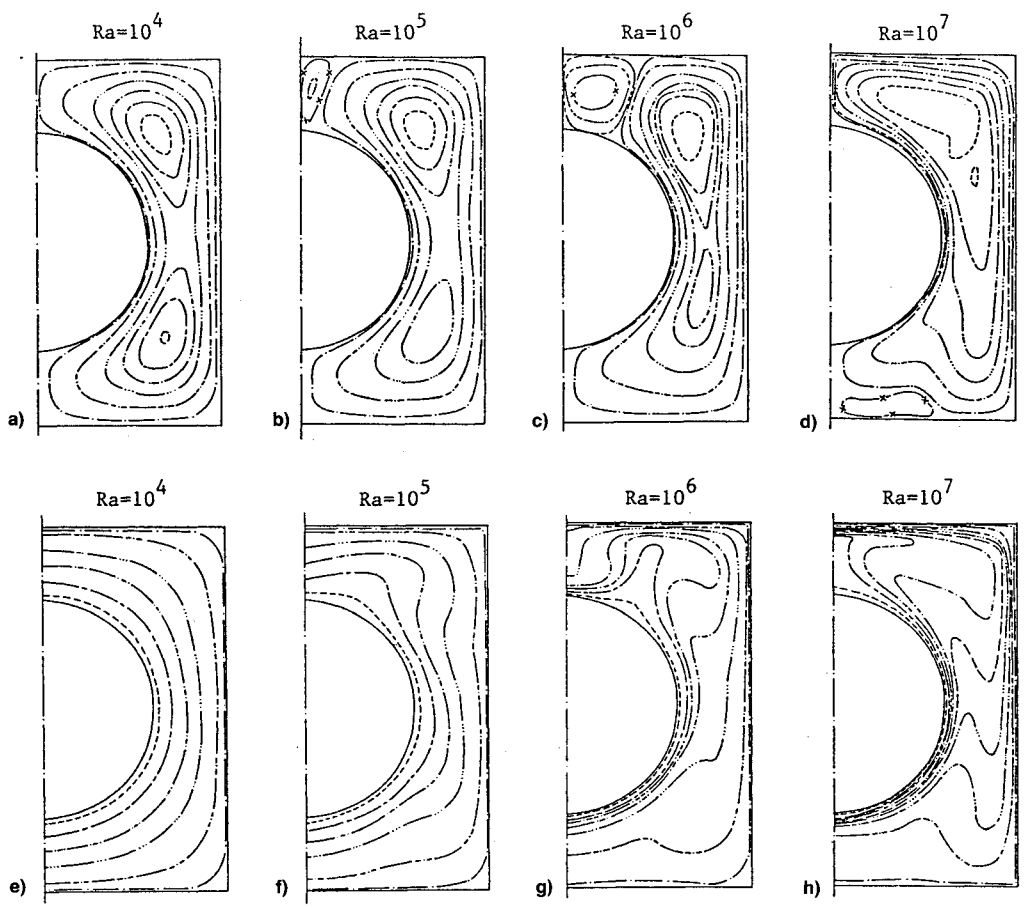


**Fig. 4 Streamline and isotherm plots ($R/L$ = 0.3).**

top of the cylinder, and forms a thermal plume. This can be seen in the streamline plots and in the isotherm contours where the isotherms move rapidly away from the inner wall near the top. For the highest aspect ratio considered ($R/L$ = 0.3), and for $Ra = 10^6$ and $10^7$, the isotherm patterns are distorted (Figs. 4f and 4g), reflecting flow separation on top (Figs. 4b and 4c). Flow separation in the upper regions of the annulus has been observed experimentally by Warrington and Powe[9] for natural convection between a cylindrical body and its cubical enclosure, and by Powe et al.[15] for natural convection between a body and its spherical enclosure. However, for a rhombic annuli (Ref. 16), no such separation was noted.

At the lower Rayleigh number ($Ra = 10^4$) studied, and for all aspect ratios considered, a relatively weak convective flow exists in the cavity, and the flow patterns (Figs. 2a, 3a, and 4a) and temperature distributions (Figs. 2e, 3e, and 4e) tend to be symmetrical across the horizontal diagonal of the enclosure. This symmetry is observed to decrease with decreasing $R/L$ values. At higher Rayleigh numbers, the isotherm and flow patterns become unsymmetrical about the horizontal diagonal, and as previously noted, the eye of the recirculating eddy moves upwards and outwards towards the cold wall. This behavior is because of, in part, the thermal stratification effects in the lower regions, promoted by the significantly larger area of the cold surface relative to the area of the hot surface. Because of this stratification, which increases with Rayleigh number, the flow cannot easily penetrate the lower region, and as seen in Figs. 2c, 2d; 3c, 3d; and 4c, 4d, the flow in this region is weak. A manifestation of this strong stratification, at $Ra = 10^7$, is the flow separation at the bottom of the enclosure (Figs. 3d and 4d). In the upper half, because of the steep destabilizing temperature gradients created by the cold surface that meets the hot fluid rising from the hot cylinder, stratification is not significant and a strong recirculating flow is obtained.

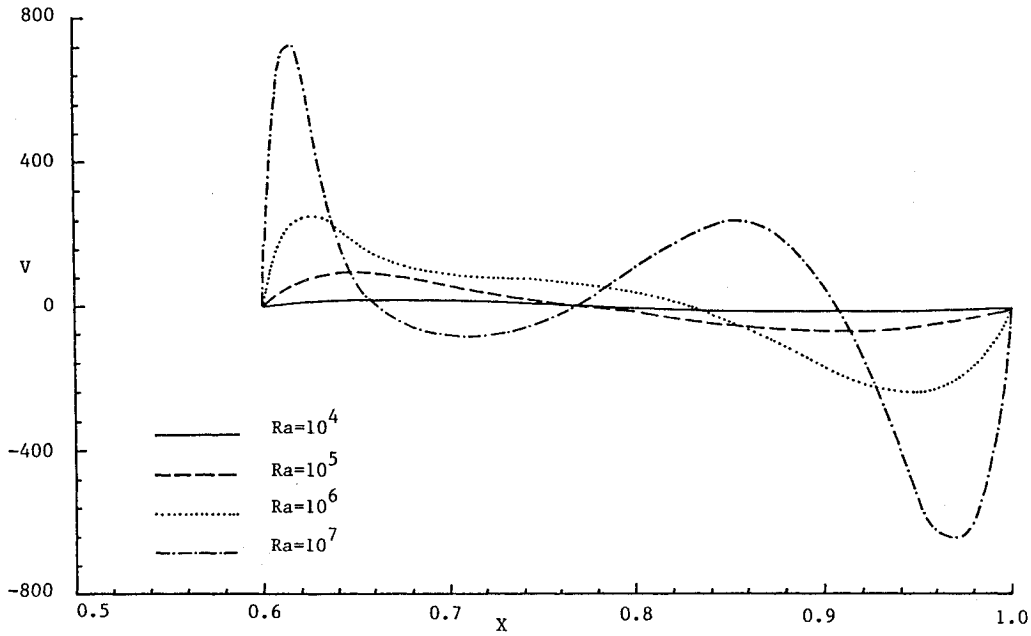


**Fig. 5 Midheight vertical velocity profiles ($R/L$ = 0.1).**

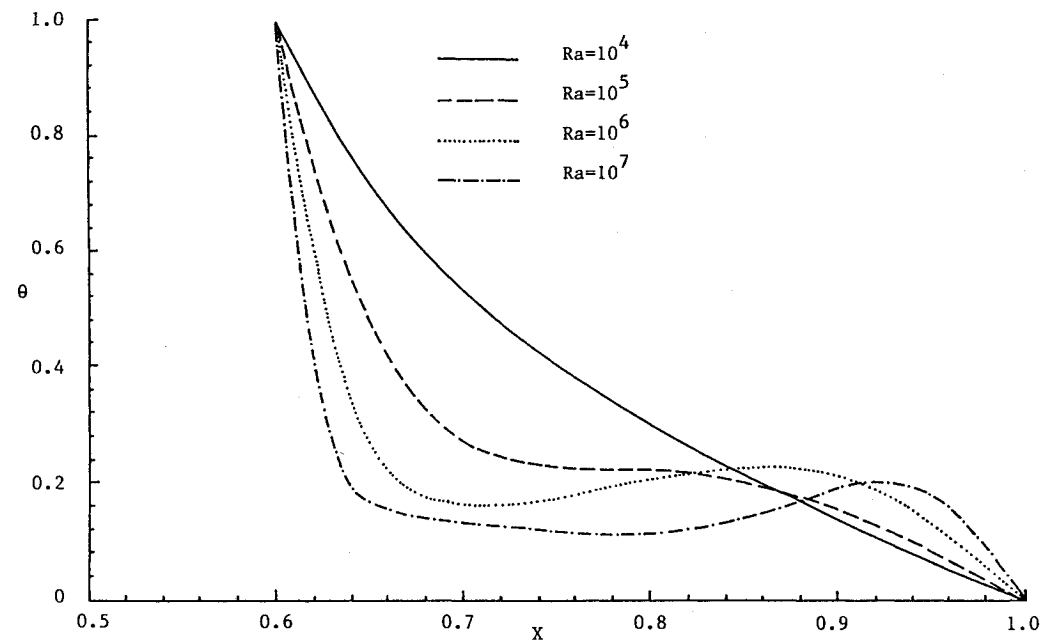


**Fig. 6 Midheight temperature profiles ($R/L$ = 0.1).**

Increasing $R/L$ produces two counteracting effects, with the greater surface area enhancing the heat transfer and buoyancy-induced convection, but at the same time adding to the viscous retardation. As shown in Table 1, the strength of the flow (indicated by ($|\psi_{max}|$) decreases with increasing $R/L$ values at lower $Ra$ numbers, because of the greater viscous effects of the added surface area. However, at the higher $Ra$ numbers, the stronger buoyancy-induced motion compensates for the added viscous effects, and $\psi_{max}$ is relatively unaffected by an increase in $R/L$. For constant $R/L$ values ($|\psi_{max}|$) expectedly increases with increasing Rayleigh number.

The phenomenon of temperature inversion, which indicates that fluid in the region close to the inner surface is cooler than that close to the colder outer surface, is observed at high Rayleigh numbers (see Fig. 4). The extent of temperature inversion is seen to be much higher for lower $R/L$ ratios because of the enhanced natural convection at lower $R/L$ values.

**Velocity and Temperature Profiles**

The vertical velocity component and the temperature profile along the horizontal centerline are shown in Figs. 5 and 6, respectively, for $R/L = 0.1$. The velocity profiles are steeper near the hot wall than that near the cold wall because of the stratification effects in the lower part of the enclosure that opposes the descending flow along the cooled surface. Note the inversions in the velocity profile at $Ra = 10^7$, which lead to corresponding inversions in the temperature profile at the higher Rayleigh number (Fig. 6). As for the velocity gradients, at the higher $Ra$ numbers, the temperature gradients are much higher in the vicinity of the hot wall.

**Nusselt Numbers**

The following relations are used to calculate the local and average heat transfer coefficients and Nusselt numbers at the inner and outer walls:

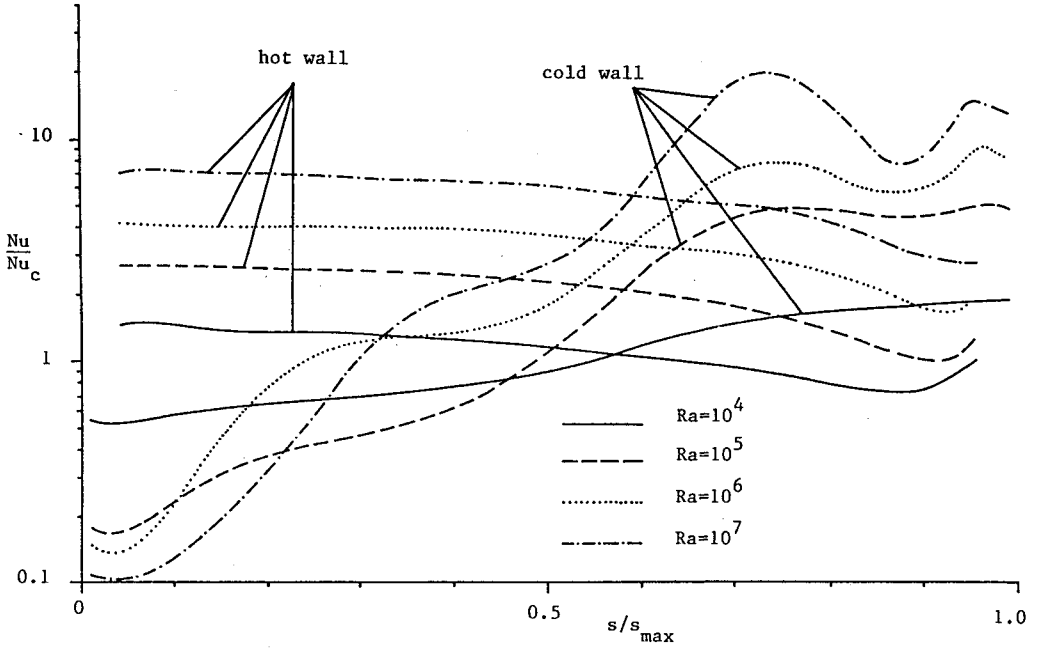


**Fig. 7 Local Nusselt number distribution along the hot and cold walls ($R/L = 0.1$).**

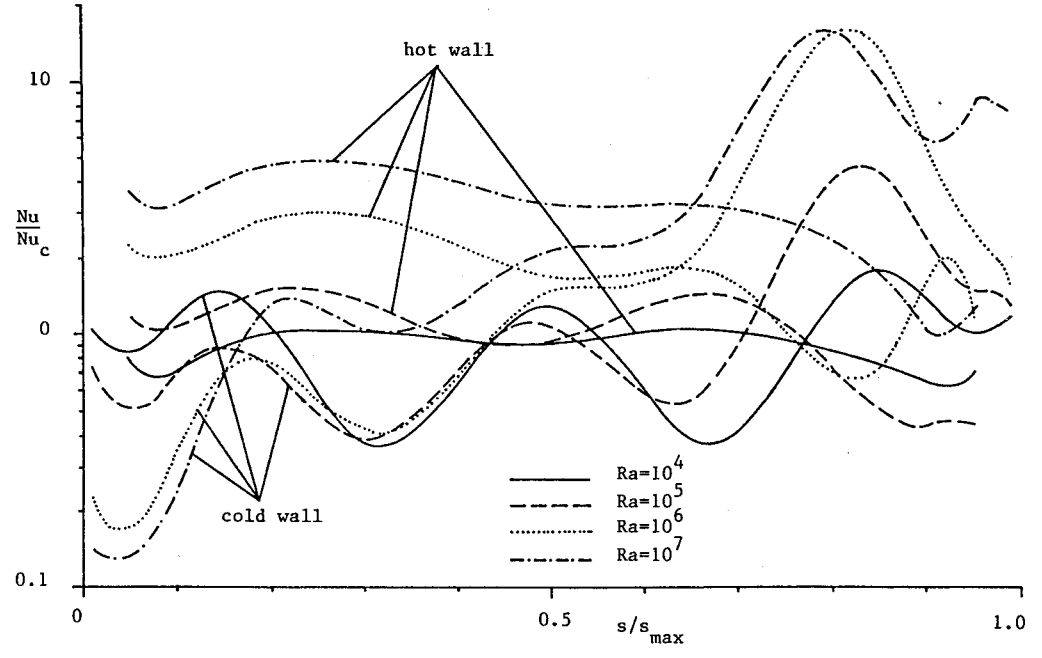


**Fig. 8 Local Nusselt number distribution along the hot and cold walls ($R/L = 0.3$).**

$$h_i = -\left[k\left.\frac{\partial T}{\partial n}\right|_i \Big/ (T_i - T_o)\right], \qquad h_o = -\left[k\left.\frac{\partial T}{\partial n}\right|_o \Big/ (T_i - T_o)\right] \tag{8}$$

$$\overline{Nu}_i = \bar{h}_i s_{i,\max}/k, \qquad \overline{Nu}_o = \bar{h}_o s_{o,\max}/k \tag{9}$$

where $n$ denotes the normal distance from the wall, and $s_{i,\max}$ and $s_{o,\max}$ are the length of the inner and outer walls, respectively. Since at steady state the Nusselt numbers along the inner and outer walls are the same, there is no need to give separate attention to $\overline{Nu}_i$ and $\overline{Nu}_o$, and attention will subsequently be focused on $\overline{Nu}$.

The normalized local Nusselt number distributions ($Nu/Nu_c$, where $Nu_c$ is the value of Nusselt number for pure conduction, i.e., $Ra = 0$) along the hot and cold walls are presented for $R/L$ values of 0.1 and 0.3 in Figs. 7 and 8, respectively. In this normalized form, the relative effect of convection can directly be assessed. Values are plotted as a function of $s/s_{\max}$ where $s$ is distance along the wall measured from its lowest point and $s_{\max}$ is the maximum possible length.

In Fig. 7, for $R/L$ of 0.1, the convection contribution to the total heat transfer along the inner hot wall increases with increasing Rayleigh number. Further, at constant Rayleigh number values, the largest normalized Nusselt numbers occur in the leading regions of the hot wall ($s = 0$). Note that the profiles are relatively flat along the hot surface. This seems to be in contrast to the observed behavior for a cylindrical annuli and is probably because of the stronger stratification effects in the lower regions of the present geometry.

Along the outer cooled wall, the normalized Nusselt number profiles are similar for all Rayleigh number values considered. In the lower half of the enclosure, conduction is the dominant heat transfer mode ($Nu/Nu_c < 1$). For $s/s_{\max} < 0.1$, the Nusselt number decreases with increasing Rayleigh number. This is because of the higher thermal stratification at a higher Rayleigh number that prohibits penetration of the flow into the lower part of the enclosure. In the upper part, convection is the dominant heat transfer mechanism ($Nu/Nu_c > 1$), and its contribution to the total heat transfer increases with increasing Rayleigh number because of the stronger convective motion of the flow. A maximum is observed in the upper region and is because of the hot fluid from the inner wall rising upwards and impinging on the cold upper wall, thereby increasing convection heat transfer.

The normalized Nusselt number profiles for an enclosure aspect ratio of 0.3 are depicted in Fig. 8. At the lowest Rayleigh number value considered, the profiles are nearly symmetrical, reflecting the effects of the more symmetrical flow pattern and isotherms at higher $R/L$ values as shown in Figs. 4a and 4e. For $Ra = 10^5$ and $10^6$, a local decrease in the heat transfer is observed near the top of the inner and outer cylinders because of separation of the flow, as shown in Figs. 4b and 4c. Otherwise, the general trend of results shows a similar behavior as in Fig. 7.

The average Nusselt number values for all cases studied are given in Table 2. At the lower Rayleigh numbers, the overall heat transfer appears to be strongly dominated by conduction. Beyond a critical Rayleigh number (which appears to be close to $10^4$ for all aspect ratios considered), convection effects become important on the total heat transfer. At constant $R/L$ values, the average Nusselt number increases with increasing

**Table 2 Average Nusselt number values**

| | $R/L$ | | |
|---|---|---|---|
| $Ra$ | 0.1 | 0.2 | 0.3 |
| 0 | 1.836 | 3.26 | 5.369 |
| $10^4$ | 2.071 | 3.331 | 5.826 |
| $10^5$ | 3.825 | 5.08 | 6.212 |
| $10^6$ | 6.107 | 9.374 | 11.62 |
| $10^7$ | 10.255 | 15.79 | 19.19 |

**Table 3 Experimental data[9] and numerical results**

| $Ra$ | $Ra_L$ | $Nu$ | $Nu_L$ | $(Nu)_{exp}$ | Difference, % |
|---|---|---|---|---|---|
| | | $R/L = 0.2$ | | | |
| $10^4$ | $1.114 \times 10^4$ | 3.331 | 5.49 | 5.286 | 3.86 |
| $10^5$ | $1.114 \times 10^5$ | 5.08 | 8.377 | 8.67 | 3.38 |
| $10^6$ | $1.114 \times 10^6$ | 9.374 | 15.4 | 14.2288 | 8.23 |
| $10^7$ | $1.114 \times 10^7$ | 15.79 | 26.03 | 23.34 | 11.52 |
| | | $R/L = 0.3$ | | | |
| $10^4$ | $0.845 \times 10^4$ | 5.826 | 5.826 | 4.26 | 36.76 |
| $10^5$ | $0.845 \times 10^5$ | 6.282 | 6.282 | 6.8 | 7.62 |
| $10^6$ | $0.845 \times 10^6$ | 11.62 | 11.62 | 10.855 | 7.05 |
| $10^7$ | $0.845 \times 10^7$ | 19.19 | 19.19 | 17.32 | 10.8 |

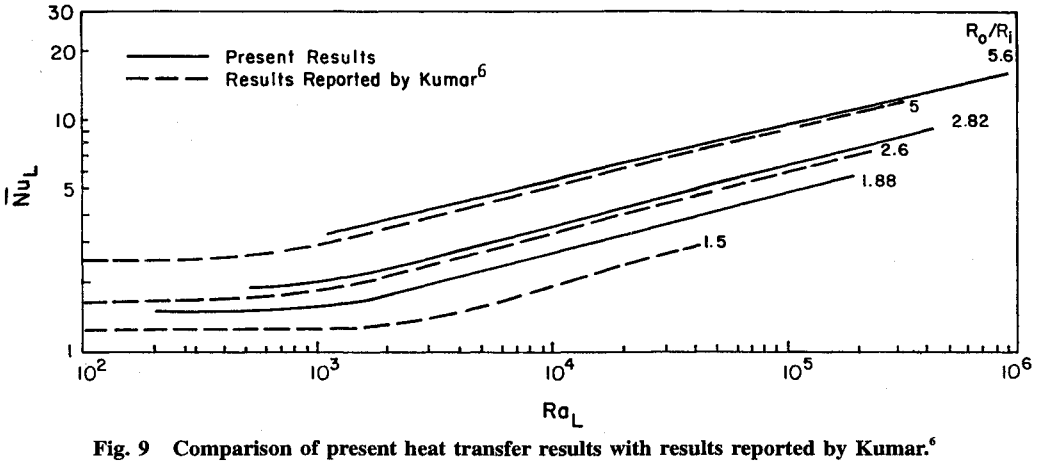


**Fig. 9 Comparison of present heat transfer results with results reported by Kumar.[6]**

Rayleigh number because of the increase in the magnitude of the buoyancy forces. When Rayleigh number is held constant, $\overline{Nu}$ increases with increasing $R/L$ values, because of the increased heat transfer surface area associated with higher $R/L$ values. For convection-dominated flows ($10^5 \leq Ra \leq 10^7$), the average Nusselt number correlation is expressed as $\overline{Nu} = 0.92Ra^{0.23}(R/L)^{0.57}$, with a maximum deviation of $\pm 8\%$. Note that the exponent of the $Ra$ number matches with the 0.23 exponent in the correlation proposed by Warrington and Powe.[9]

### Comparison with Published Experimental and Numerical Results

A literature survey was performed in an attempt to find experimental results for the problem studied. Unfortunately, no data exactly describing the problem seemed available. In view of this, generated results are compared in this section against the published experimental data of Warrington and Powe[9] and the numerical data of Kumar.[6] These two configurations are deemed to approximate the present problem.

Warrington and Powe[9] have presented experimental natural convection heat transfer results between a cylindrical body and its cubical enclosure. Thus, an attempt is made here to compare two-dimensional numerical predictions to three-dimensional experimental data. The experimental average Nusselt number results for $R/L$ values of 0.2143 and 0.333 are compared against the present average Nusselt number values for $R/L$ of 0.2 and 0.3, respectively. Warrington and Powe define the Rayleigh and Nusselt numbers based on a hypothetical gap width $L = R_o - R_i$, calculated as the distance from an imaginary outer sphere whose volume is equal to the volume of a cube, to an imaginary inner sphere whose volume is equal to the volume of the inner body. The present values of Rayleigh and Nusselt numbers recomputed using the definitions of Warrington and Powe along with the corresponding experimental data are displayed in Table 3 for aspect ratios of 0.2 and 0.3, respectively. Keeping in mind the slight difference between the aspect ratios in the two studies, and the three-dimensional effects present in the experimental study, the present predictions compare very well with the experimental results. Only for $R/L = 0.3$ and $Ra_L \cong 10^4$, the two results do not agree as well.

Warrington and Powe[9] showed that the effects of the enclosure shape on the total heat transfer is small. Based on this claim, the present results are also compared with the numerical predictions of Kumar[6] for natural convection between concentric horizontal cylinders. Again, the Rayleigh and Nusselt numbers are based on a hypothetical gap width, $L = R_o - R_i$, defined now (because of the two-dimensional nature of the problem) as the distance from an imaginary outer cylinder whose area is equal to the area of a square to the inner cylinder. The aspect ratios of 0.1, 0.2, and 0.3 correspond to $R_o/R_i = 5.6$, 2.82, and 1.88, respectively, and are compared against results for which $R_o/R_i = 5$, 2.6, and 1.5. The comparison is shown in Fig. 9, and once again, satisfactory agreement of the present predictions with the predictions of Kumar is obtained.

## Concluding Remarks

A numerical study of natural convection heat transfer from an isothermal heated inner cylinder to its square cooled enclosure is performed. At low Rayleigh number values, the flow is weak and conduction is the dominant heat transfer mode. At high Rayleigh number values, convection dominates the scene and promotes thermal stratification in the lower half of the enclosure. The dominant feature of the flow is a recirculating eddy with its center moving upwards and outwards towards the upper portion of the cold wall with increasing Rayleigh number. As the gap between the inner and outer surfaces decreases, there is a reduction of the flow strength, the thermal stratification, and the asymmetry between the upper and lower halves. Separation above the inner cylinder is observed for the highest $R/L$ values considered. The local Nusselt number shows trends that are different from that observed in cylindrical or rhombic annuli. Along the heated wall, a flat Nusselt number profile is obtained while along the cooled wall, the profile shows the expected peak near the top, but decays to values smaller than the conduction values near the bottom. The predicted values of the average Nusselt number, however, compare well with previously published data for similar geometries.

## Acknowledgment

The financial support provided by the University Research Board of the American University of Beirut through Grant 113040-48756 is gratefully acknowledged.

## References

[1]Kuehn, T. H., and Goldstein, R. J., "An Experimental and Theoretical Study of Natural Convection in the Annulus Between Horizontal Concentric Cylinders," *Journal of Fluid Mechanics*, Vol. 74, 1976, pp. 695–795.

[2]Custer, J. R., and Shaughnessy, E. J., "Thermoconvective Motion of Low Prandtl Number Fluids Within a Horizontal Cylindrical Annulus," *Journal of Heat Transfer*, Vol. 99, 1977, pp. 596–602.

[3]Farouk, B., and Guceri, S. I., "Laminar and Turbulent Natural Convection in the Annulus Between Horizontal Concentric Cylinders," *Journal of Heat Transfer*, Vol. 104, No. 4, 1982, pp. 631–636.

[4]Bubnovich, V. I., and Kolesnikov, P. M., "Conjugate Unsteady-State Heat Transfer During Laminar Natural Convection in a Horizontal Annulus," *Journal of Engineering Physics*, Vol. 51, No. 4, 1986, pp. 576–583.

[5]Kolesnikov, P. M., and Bubnovich, V. I., "Non-Stationary Conjugate Free-Convective Heat Transfer In Horizontal Cylindrical Coaxial Channels," *International Journal of Heat and Mass Transfer*, Vol. 31, No. 6, 1988, pp. 1149–1156.

[6]Kumar, R., "Study of Natural Convection in Horizontal Annuli," *International Journal of Heat and Mass Transfer*, Vol. 31, No. 6, 1988, pp. 1137–1148.

[7]Chang, K. S., Won, Y. H., and Cho, C. H., "Patterns of Natural Convection Around a Square Cylinder in a Horizontal Circular Cylinder," *Journal of Heat Transfer*, Vol. 105, No. 2, 1983, pp. 273–280.

[8]Oosthuizen, P. H., and Paul, J. T., "Finite Element Study of Natural Convection Heat Transfer from a Prismatic Cylinder in an Enclosure," *Numerical Methods in Heat Transfer*, Vol. 62, 1987, pp. 13–21.

[9]Warrington, R. O., and Powe, R. E., "The Heat Transfer of Heat by Natural Convection Between Bodies and Their Enclosures," *International Journal of Heat and Mass Transfer*, Vol. 28, No. 2, 1985, pp. 319–330.

[10]Warrington, R. O., Brown, P. K., and Powe, R. E., "Natural Convection Heat Transfer Within Enclosures at Reduced Pressures," *Proceedings of the 8th International Heat Transfer Conference*, Vol. 4, 1986, pp. 1483–1488.

[11]Ghaddar, N. K., "Natural Convection Heat Transfer Between a Uniformly Heated Cylindrical Element and Its Rectangular Enclosure," *International Journal of Heat and Mass Transfer*, Vol. 35, No. 10, 1992, pp. 2327–2334.

[12]Thompson, J. F., *Numerical Grid Generation*, North-Holland, Amsterdam, 1982.

[13]Patankar, S. V., *Numerical Heat Transfer and Fluid Flow*, Hemisphere, New York, 1980.

[14]Rhie, C. M., and Chow, W. L., "Numerical Study of the Turbulent Flow Past an Airfoil with Trailing Edge Separation," *AIAA Journal*, Vol. 21, No. 11, 1983, pp. 1525–1532.

[15]Powe, R. E., Baughman, R. C., Scanlan, J. A., and Teng, J. T., "Free Convective Flow Patterns Between a Body and Its Spherical Enclosure," *Transactions of the American Society of Mechanical Engineers, Series C, Journal of Heat Transfer*, Vol. 97, 1975, pp. 296–298.

[16]Moukalled, F., Diab, H., and Acharya, S., "Numerical Simulation of Laminar Natural Convection in Concentric Ducts of Rhombic Cross-Sections," *Numerical Heat Transfer*, Vol. 24, No. 1, 1993, pp. 101–119.